E15-2004-65

NEW RESULTS IN STUDYING OF THE COLLINEAR CLUSTER TRIPARTITION OF THE ^{252}Cf NUCLEUS

Reported at the V International Seminar on Fission,
16–19 September 2003, Pont d'Oye, Belgium
and at the XVI International Workshop on Physics of Nuclear Fission,
7–10 October 2003, Obninsk, Russia

Yu. V. Pyatkov[1,2], D. V. Kamanin[2], W. Trzaska[3], S. R. Yamaletdinov[3], E. A. Sokol[2],
A. N. Tjukavkin[1,2], A. A. Aleksandrov[2], I. A. Aleksandrova[2], S. V. Denisov[2], V. P. Krajnov[4],
S. V. Khlebnikov[5], T. E. Kuzmina[5], E. A. Kuznetsova[2], S. V. Mitrofanov[2],
Yu. E. Penionzhkevich[2], Yu. V. Ryabov[6], V. G. Tishchenko[2], B. V. Florko[2]

[1]Moscow Engineering Physics Institute, 115409 Moscow, Russia
[2]Joint Institute for Nuclear Research, 141980 Dubna, Russia
[3]Department of Physics, University of Jyväskylä, FIN-40014 Jyväskylä, Finland
[4]Moscow Technical Physics Institute, 141700 Dolgoprudnij, Russia
[5]Khlopin Radium Institute, 194021 St. Petersburg, Russia
[6]Institute for Nuclear Research RAN, 117312 Moscow, Russia

Пятков Ю. В. и др. E15-2004-65
Новые результаты в изучении тройного коллинеарного кластерного распада в спонтанном делении ^{252}Cf

На модифицированном спектрометре ФОБОС получены новые экспериментальные результаты, подтверждающие наличие канала тройного коллинеарного кластерного распада (ТККР) спонтанно делящегося ядра ^{252}Cf. Обнаружены события с малой полной массой делительных фрагментов, которая оказалась на 30–40 % меньше начальной массы делящегося ядра. Группа этих редких событий при условии большой измеренной нейтронной множественности обнаружила специфические структуры в матрице масс коллинеарных осколков деления в виде прямоугольников, ограниченных магическими массовыми числами.

Работа выполнена в Лаборатории ядерных реакций им. Г. Н. Флерова ОИЯИ.

Препринт Объединенного института ядерных исследований. Дубна, 2004

Pyatkov Yu. V. et al. E15-2004-65
New Results in Studying of the Collinear Cluster Tripartition of the ^{252}Cf Nucleus

New experimental results confirming collinear cluster tripartition mode in ^{252}Cf (sf) have been obtained at the modified FOBOS spectrometer. Some events have been detected with the low total mass of fission fragments, which turned out to be by 30–40 % smaller than the initial mass of the fissioning nuclei. The group of these rare events gated by the large neutron multiplicity measured revealed the specific rectangular-shaped structures in the mass distribution of the coincident collinear fragments bounded by the magic mass numbers.

The investigation has been performed at the Flerov Laboratory of Nuclear Reactions, JINR.

Preprint of the Joint Institute for Nuclear Research. Dubna, 2004

INTRODUCTION

In our previous works [1–3] we have discussed the experimental indications of a new type of nuclear transformation called by us «collinear cluster tripartition» (CCT) due to the special features of such events observed at the yield level of $\sim 10^{-5}$–10^{-6} with respect to conventional binary fission of the ^{248}Cm and ^{252}Cf nuclei. The total mass of two complementary fragments amounted to about 70% of the initial mass of the fissioning nuclei. Mass-energy correlations for these rare events allow one to associate them with the decay of the system via an elongated three-body chain-like configuration. Two fragments originating at the outmost left and the outmost right positions fly apart along the chain axis, i.e. collinear, while the middle fragment can stay almost at rest. At least one of the detected fragments formed in each event under discussion is a magic nucleus by its composition (i.e. cluster by definition).

The experiments have been performed at the 4π-spectrometer FOBOS installed at the FLNR of the JINR [4]. In order to improve reliability of identification of the CCT events the FOBOS setup has been recently equipped with the neutron detectors and with the special symmetric start detector [5]. The data processing procedure has been modified as well. The preliminary results of the new set of experiments at the modified FOBOS spectrometer have been presented in [6]. We discuss in this paper some obtained results in some detail.

The problem of «true ternary fission» has a long history. Multiple attempts (for instance, the most famous [7, 8]) to discover such a decay channel for low excited nuclei did not succeed so far. It should be stressed that the ternary decay (CCT) mentioned above could not be detected in the framework of the experimental approaches developed in the past. Except of the radio-chemical and mass-spectrometric techniques, being selective to revealed nuclides, all the experiments performed aimed at detecting three moving fragments emitted at some angles to each other (equal angles for equal fragments). Such events could be expected from the symmetry point of view, however, such an experimental design contradicts to the theoretical estimations. Within the liquid drop approach [9] and, recently, in its extended version [10], it was shown that the chain-like (prolate) configuration is preferred compared to oblate shapes. As for ternary fission it is quite understandable bearing in mind the higher Coulomb component of the potential barrier has to be overcome for the triple decay. The existence of an elongated (prolate) configuration with two necks for the fissioning Cf nucleus was demonstrated recently in our work [6], where the shell corrections were taken

into account as well. The results of searching for CCT in spontaneously fissioning nuclei were reported almost simultaneously by us [1] (revealing the effect for the ^{248}Cm and, subsequently, for the ^{252}Cf nucleus) and in [11] (here the absence of the effect at the level of 10^{-5} with respect to binary fission of the ^{252}Cf nucleus is reported).

1. EXPERIMENTAL TECHNIQUE

The experimental layout of the modified FOBOS spectrometer is shown in Fig.1.

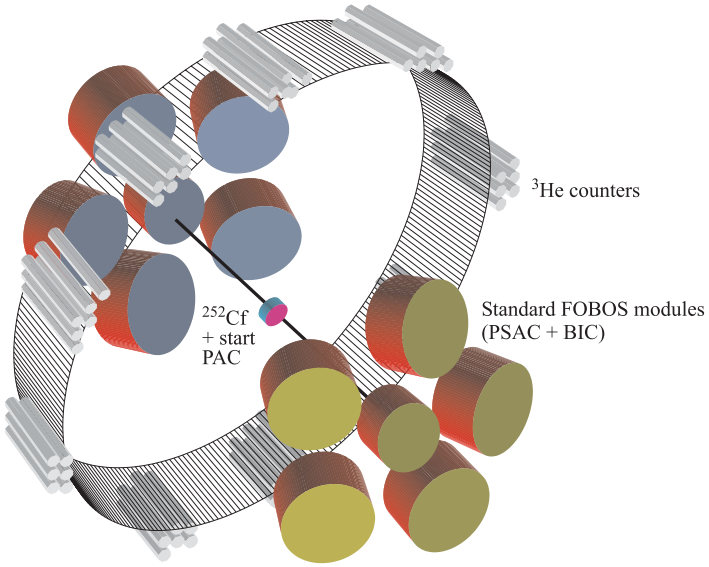

Fig. 1. Schematic view of the modified FOBOS setup. The spontaneous fission source is placed inside of the start detector at the geometrical center of the spectrometer. The belt consisting of 140 ^{3}He neutron counters is placed perpendicular to the mean fission axis of the registered fragments which are detected by 12 standard FOBOS modules consisting of the position-sensitive avalanche counters (TOF) and the Bragg ionization chambers (BIC)

Two groups of detectors containing five big and one small FOBOS modules each, were used as a double-armed TOF-E (time-of-flight-energy) spectrometer which covered $\sim$29% of the hemisphere in each arm, and thus the energies and the velocity vectors of the coincident fragments were detected. The neutron detector consisted of 140 separate hexagonal modules comprising ^{3}He-filled proportional

counters in a moderator, this covered altogether $\sim$19% of the complete solid angle of 4π. The electronics of the «neutron belt» was operated in the slave mode being triggered by the event selector of the gas part of the FOBOS detector. The number of triggered ^{3}He neutron counters was added to the data stream as an additional parameter for each registered fission event.

2. CALIBRATION PROCEDURE

The precise reconstruction of the fragment masses taking into account large energy losses in the foils of the gas detectors is obstructed by imperfect energy loss tabulations which are apparent in our previous data as some asymmetry in the mass-mass correlations of the events. This has enforced an improvement of the calibration procedure. The latter is extremely important for the discussion on data reliability, therefore, its detailed description is given below.

The TOF calibration has been performed by means of fitting the experimental mass of binary fission distribution to that known from [12]. The free parameters of the fit were the effective thickness of an adsorbing matter on the particle flight-path and the time calibration constants. The mass spectrum $Y(M_{\rm tt})$ shown in Fig. 2 reproduces well the positions of gravity centers of the light and heavy peaks and the width of each distribution. An additional check of the mass calibration has been performed by comparing the velocity distribution with the known data [12]. Here a good agreement is observed as well (Fig. 3).

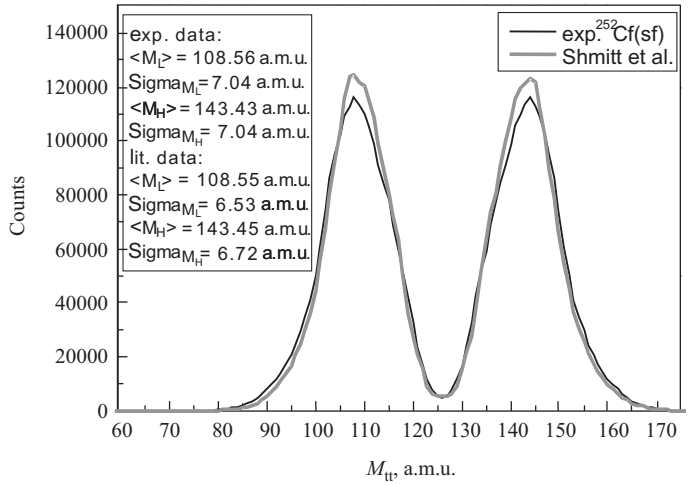

Fig. 2. Comparison of the mass spectrum of the fission fragments of ^{252}Cf(sf) obtained by the TOF-TOF analysis $M_{\rm tt}$ with that taken from Ref. [12]

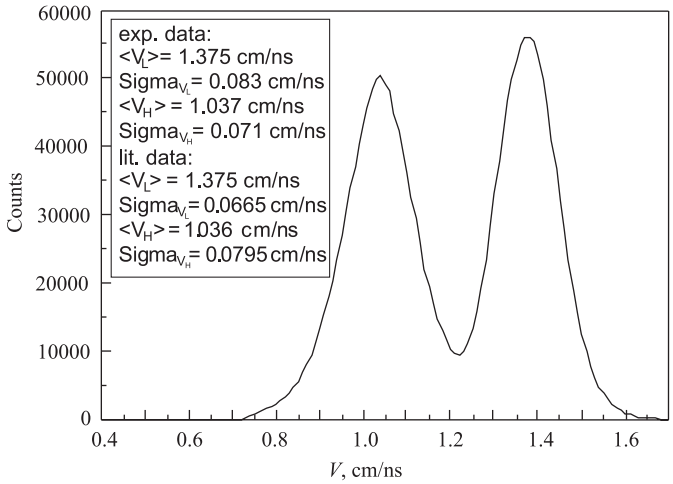

Fig. 3. The experimental spectrum of the velocity of the ^{252}Cf(sf) fission fragments. The average values for comparison are also given in the inset [12]

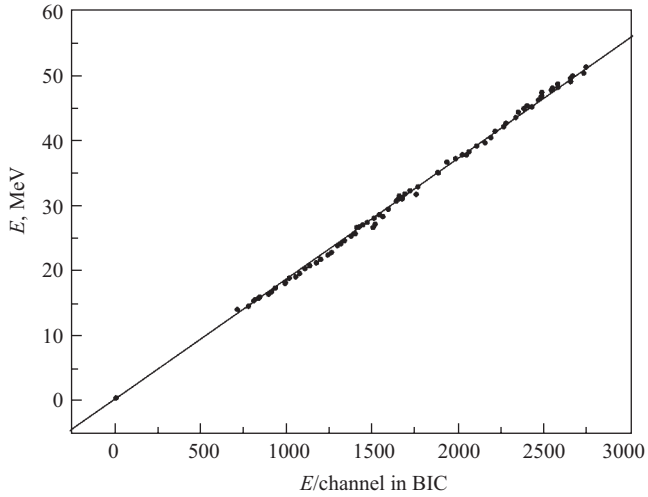

Fig. 4. The correlation obtained between the raw energy signals in the Bragg chamber (in channels) and the FF energy (in MeV) calculated from the TOF-TOF analysis corrected for the post-fission neutrons and for the entrance foils

In order to improve the mass calibration in the framework of the TOF-E method the procedure aimed to restore the fragment energy has been refined. This task is especially difficult for the slow CCT fragments since they lose up to 70% of their initial energy before entering the gas volume. The final mass spectrum obtained by the TOF-E analysis is given further in Fig. 7. The mass resolution achieved using the TOF-E method is found to be much worse than the corresponding value obtained by the TOF-TOF analysis. In case of incomplete kinematics, e.g. for the CCT events, the TOF-TOF method becomes unusable since it exploits the momentum conservation law of the binary reaction products. Taking into account that the middle nonobservable fragment corresponds to almost the third part of the initial mass the detection of such a large mass deficit does not require perfect mass resolution.

On the other hand, any systematical shift in the mass calibration must be excluded for the correct physical conclusions on the CCT mechanism. Our efforts in improving the transport calculations has resulted in the perfect correlation (Fig. 4) between the measured energy in the Bragg chamber (in channels) and the estimated one (in MeV). Such a straight line dependence could be accepted as the calibration only if both the used energy-loss table [13] is correct and if there is no significant amplitude defect in the ionization chamber what is exactly the case.

The correlation line obtained crosses the point of origin and thus additionally confirms quality of the calibration, because this constraint automatically follows from the algorithm the Bragg processor uses to integrate the fragment-track charge in the chamber [4]. This linear dependence means that the energy calibration is unambiguous and non-shifted. This becomes essential for searching for the CCT fragments with their unusual mass-to-energy ratio.

3. RECONSTRUCTION OF THE FRAGMENT MASS

After implementation of the energy calibration described above both the velocity of fragment before entering the BIC and its energy deposited in the gas volume become known. The mass of the fragment is derived from these quantities according to the following algorithm illustrated in Fig. 5. There the dependence of the energy on the fragment mass M deposited in the BIC $E_{\rm cal}\,(M|V = {\rm const})$ for the different fixed velocities V before entering the BIC are presented (for instance, 1.4 cm/ns, see the upper curve). Then one calculates actually the total energy $E_{\rm in}$ of the fragment with the given mass M and its velocity V. The energy $E_{\rm cal}$ of the fragment after crossing of the entrance window of the BIC is obtained by calculating the energy loss applying the corresponding table [13]. Let us assume $E_{\rm ch}$ to be the energy of the fragment deposited in the BIC and $V_{\rm in}$, its actual velocity

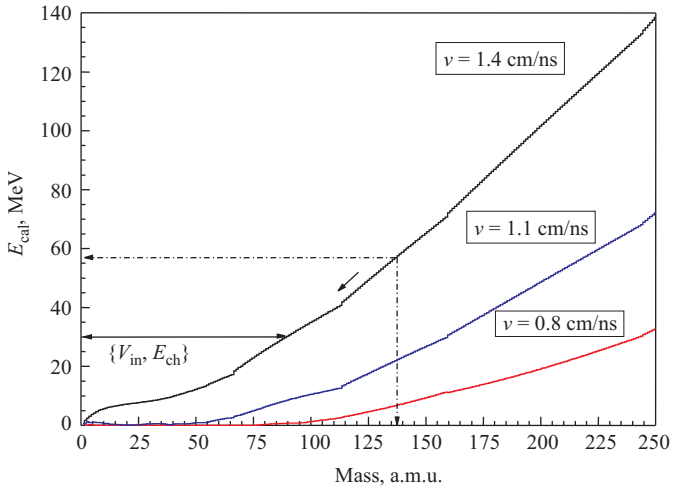

Fig. 5. Illustration of the mass reconstruction procedure

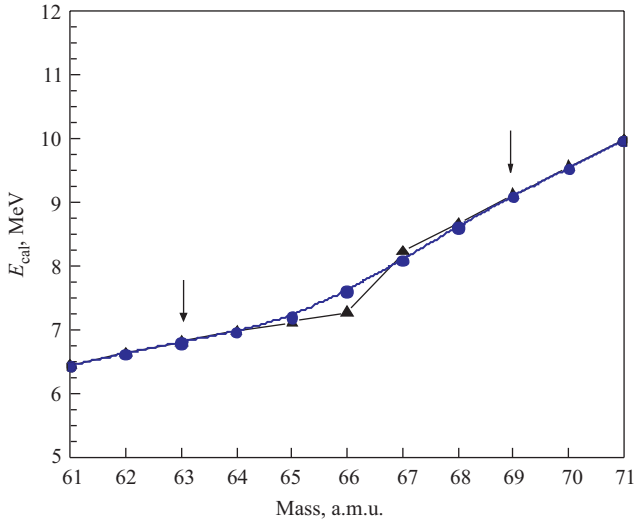

Fig. 6. Smoothing of gaps in the table of energy losses. The values calculated using the initial tabulations are shown by triangles; the smoothed ones are shown by circles. Arrows mark the points of «stitching» of the initial $E_{\rm cal}$ $(M|V = \text{const})$ dependence with the smoothed one

before the BIC entrance. In order to restore its mass we examine mass-by-mass descending along the curve $V_{\rm in} = {\rm const}$ in Fig. 5 until the following condition is met for the first time:

$$E_{\rm ch} < E_{\rm cal}(M|V_{\rm in}).$$

This procedure is complicated by some discontinuities in the energy loss calculation giving the function $E_{\rm cal}(M,V)$ caused by imperfect energy losses tabulations as exemplified in Fig. 6 by triangles. To avoid such a gap we applied smoothing by means of a cubic polynomial patching of the initial dependence $E_{\rm cal}\ (M|V)$ in the vicinity of the gap by equalizing both the values and the first derivatives at the edges. Such a method has been proven to be the best one for this purpose. The smoothed values are shown in Fig. 6 by the circles. The mass spectrum obtained in the frame of the presented procedure is shown in Fig. 7 in comparison with the known one [14]. There are no shifts in the peak positions what is important for identification of the CCT events. This fact is demonstrated as well by Fig. 8 where the dependence $<M_{\rm te}>$ versus $M_{\rm tt}$ looks like a straight line without any offset. Here the shift due to neutron emission has been, as explained below, taken into account.

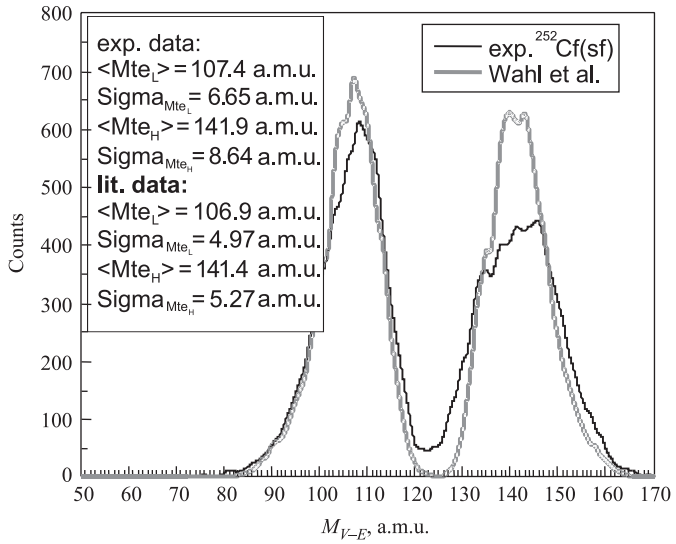

Fig. 7. Comparison of the FF mass spectrum obtained from the TOF-E analysis with the data of Ref. [14]

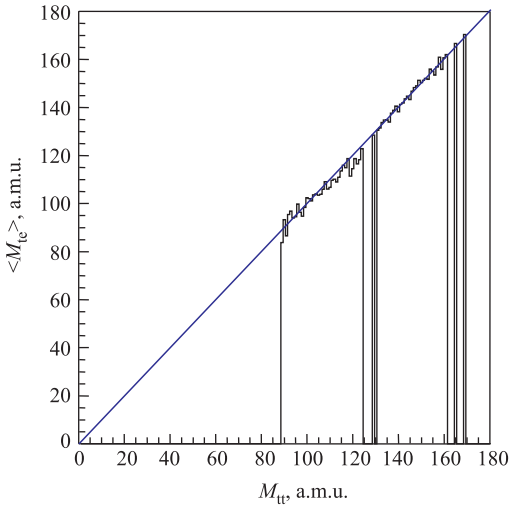

Fig. 8. The correlation between the mass $<M_{\rm te}>$ obtained in TOF-E analysis and the mass $M_{\rm tt}$ from TOF-TOF analysis

4. NUMERICAL MODEL OF THE NEUTRON REGISTRATION CHANNEL

An independent indication of the occurred CCT could be a high neutron multiplicity accompanying such an event [3]. In order to exploit this property as a sign of CCT coupled the FOBOS spectrometer was completed with the «neutron belt» mentioned before. The legitimacy of using the number of the triggered neutron counters as a measure of the true neutron multiplicity under certain experimental conditions determined by the registration efficiency, background of any type and the decay rate has been studied in the frame of the specially developed numerical model, presented in brief in [5].

A contribution from three different sources of neutrons has been taken into account as follows:

1. From moving fission fragments originating from conventional binary fission and detected in coincidence in the opposite arms of the spectrometer. Note that the time gate of 128 μs for the registration of neutrons is opened just at the moment when the fission fragments (FF) fires the «stop» detectors (start signal).

2. The moving FF also originated from the conventional fission events occurred before the end of the time gate. This source will be named below «the random source».

3. The neutron background in the experimental hall.

The proposed model does not include any contribution of CCT as the source of neutrons. It should be observed as the difference between the experimental multiplicity distribution and the simulated one for binary events.

The probability $W(\varepsilon)_i$ of registration of i neutrons from the first source is given by the following expression [15]:

$$W(\varepsilon)_i = \sum_{k=i}^{M} \varphi_k \varepsilon^i (1-\varepsilon)^{k-i} C_k^i, \tag{1}$$

where ϕ_k is the emission probability of k neutrons known from the literature (Table 1) and ε is the detecting efficiency, M is taken as $k_{\max}$ in Table 1.

Table 1. **Probability of emission of k neutrons from ^{252}Cf(sf) [16]**

k	0	1	2	3	4	5	6	7
φ_k	0.002	0.024	0.123	0.271	0.306	0.188	0.066	0.0163

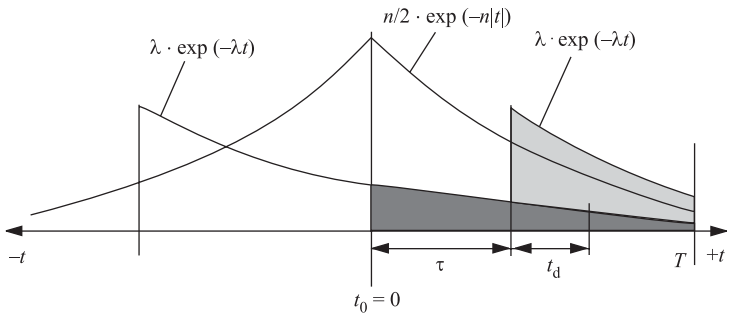

Fig. 9. Scheme illustrating a contribution of the random source in time

An influence of the second (random) source since some time t_0 (Fig. 9) is taken into account in the gate [0, T] opened for detecting neutrons after the FF coincidence. An independent fission event at any time τ is then interpreted as a random coincidence while each neutron emitted by the corresponding FF needs some time $t_{\rm d}$ to be detected. This requires the neutron to hit the detector belt covering the η-fraction of 4π. The time interval $t_{\rm d}$ is described by an exponential distribution function with the time constant λ that has been derived from the

experimental spectrum of neutron detection times. Using the well-known MCNP code we have estimated the detection efficiency f of the neutron belt for an isotropic neutron source integrated within infinite time. The value f obtained for the neutron energy of 0.5 MeV was about 60%, but it decreases slightly as the neutron energy grow up to 1 MeV. Reliability of our MCNP simulations have been checked by reproducing the experimental values of the timing constant λ chosen to be $\sim$ 20 μs. Both the simulation and the data are shown in Fig. 10.

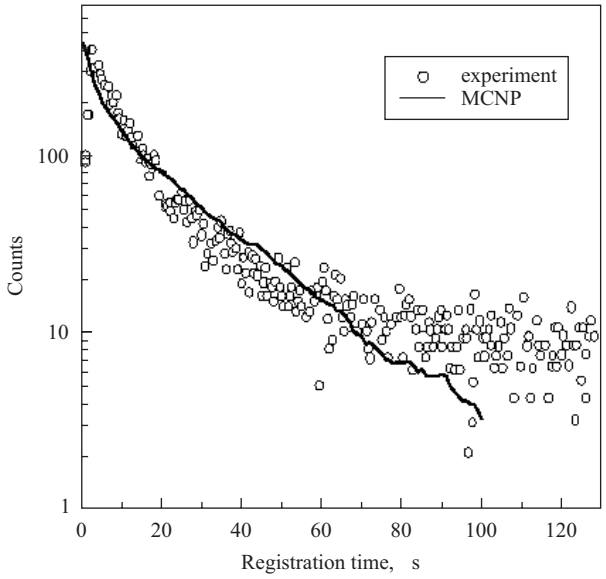

Fig. 10. Capture time for neutrons in the 16-fold detector array

The probability $P(\eta)_i$ that i neutrons reach the detector array is given by the equation

$$P(\eta)_i = \sum_{k=i}^{M} \varphi_k \eta^i (1-\eta)^{k-i} C_k^i. \qquad (2)$$

Note that the detecting efficiency degrades due to escaping of neutrons and their absorption in the moderator, and hence it is appreciably lower than the geometrical acceptance.

The probability P_λ to detect the neutron in the time interval [τ, T] is calculated according to the following expression:

$$\mathrm{P}_\lambda = \int_0^{T-\tau} \lambda \exp(-\lambda t) dt. \tag{3}$$

The probability to register «k» out of «r» (r is a multiplicity) neutrons ($r \geqslant k$) with the detector efficiency P_λ is known to be binomial. Summing up the registration probabilities multiplied by the weight function *n* exp *(-nt)* (where n is the fission rate of the source) for all other time points within the gate one takes proper account of the random neutron source. The general formula to calculate the probability of neutron registration in the interval [0, T] is

$$\phi_\nu^{l+} = \sum_{n=0}^{N} \sum_{l=\nu}^{M} \sum_{i=l}^{M} P(\eta)_k f^l (1-f)^{i-l} C_i^l \left[1 - \int_0^{T+t_n^+} \lambda \mathrm{e}^{-\lambda t} dt \right]^{l-\nu} \times \\ \times \left[\int_0^{T+t_n^+} \lambda \mathrm{e}^{-\lambda t} dt \right]^{\nu} C_l^\nu \frac{1}{2} n \mathrm{e}^{-nt}. \tag{4}$$

The above obtained function ϕ_ν^{l+} does not cover neutrons emitted earlier, i. e. before t_0 (Fig. 9). These neutrons can also be detected within the gate [0, T]. The random coincidences in the time interval [$-\infty$, 0] contribute as follows:

$$\phi_\nu^{l-} = \sum_{n=0}^{N} \sum_{l=\nu}^{M} \sum_{i=l}^{M} P(\eta)_k f^l (1-f)^{i-l} C_i^l \left[1 - \int_{|t_n^-|}^{T+|t_n^-|} \lambda \mathrm{e}^{-\lambda\left(t+|t_n^-|\right)} dt \right]^{l-\nu} \times \\ \times \left[\int_{|t_n^-|}^{T+|t_n^-|} \lambda \mathrm{e}^{-\lambda\left(t+|t_n^-|\right)} dt \right]^{\nu} C_l^\nu \frac{1}{2} n \mathrm{e}^{-nt}. \tag{5}$$

The background in the experimental hall with the intensity b which is the third neutron source obeys Poisson's distribution law

$$P^b = \frac{(bt)^k}{k!} \mathrm{e}^{-bt}. \tag{6}$$

The final distribution obtains the form

$$I_k = \sum_{\mu=0}^{K} P^b_{k-\mu} \left[\frac{\sum\limits_{\nu=0}^{\mu} \phi_{\mu-\nu} W_\nu(\varepsilon) \left[\frac{1}{2} \int\limits_0^{\tau_1} n\mathrm{e}^{-nt} dt + \frac{1}{2} \int\limits_0^{\tau_2} n\mathrm{e}^{-nt} dt \right]}{\sum\limits_{\mu=0}^{M} \sum\limits_{\nu=0}^{\mu} \phi_{\mu-\nu} W_\nu(\varepsilon)} + \right.$$

$$\left. + \frac{W_\mu(\varepsilon) \left[1 - \left(\frac{1}{2} \int\limits_0^{\tau_1} n\mathrm{e}^{-nt} dt + \frac{1}{2} \int\limits_0^{\tau_2} n\mathrm{e}^{-nt} dt \right) \right]}{\sum\limits_{\mu=0}^{M} W_\mu(\varepsilon)} \right], \quad (7)$$

where

$$\phi_\nu = \frac{\phi^{l+}_\nu + \phi^{l-}_\nu}{\sum\limits_{\nu=0}^{M} \left(\phi^{l+}_\nu + \phi^{l-}_\nu \right)}.$$

In the simulation performed for the actual intensity of the source of $n = 330\,\mathrm{s}^{-1}$ and of the neutron background of $b = 50\,\mathrm{s}^{-1}$ were substituted. The simulated I_k and experimental spectra are compared in Fig. 11. A good agreement

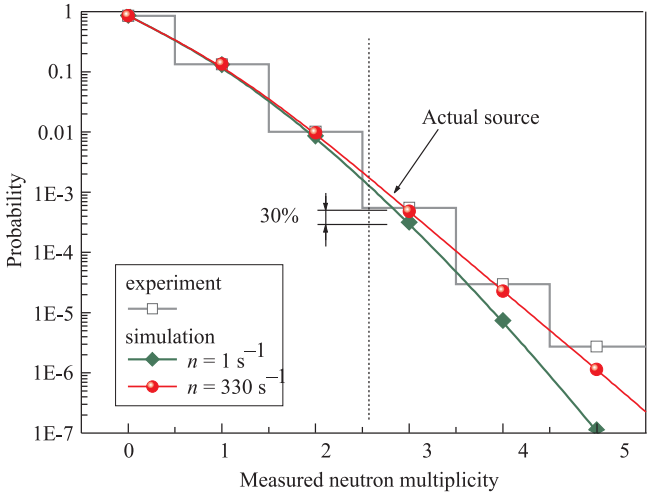

Fig. 11. Comparison of the simulated neutron multiplicity with the experimentally measured one (n is a fission rate of the source). The difference of 30% between the probability of 3-fold neutron event from the actual source used during the experiment and the free of the neutron pile up case ($n = 1$) means high reliability of the measured high-fold neutron data in searching for the true high-multiplicity events

is observed apart from the high multiplicity tail where the experimental values systematically exceed the model predictions. This discrepancy turned to be an effect expected due to the unaccounted contribution of neutrons from the CCT events.

The fraction of events with the true multiplicity above 3 amounted to 70% among those registered on conditions that three or more neutrons are detected. This important conclusion drawn with the help of our model of the neutron registration channel is also shown in Fig. 11 while $n = 1$ corresponds to lack of the random source.

5. RESULTS

The mass-mass plot of the coincident fragments with the high multiplicity of neutrons (at least three of them should be detected) is shown in Fig. 12 *a*. It is easy to recognize the rectangular-shaped structure below the locus of conventional binary fission. This structure becomes more conspicuous (Fig. 12 *b*) if the velocity cut shown in Fig. 13 is applied to the distribution. The clearing effect can be explained in the following terms.

Fragments scatter both at the electrodes of the «stop» avalanche counter and at the supporting grids of the ionization chamber that provides the main part of the faulty events which imitate the CCT effect searched for. Indeed, the mass of the heavy fragment calculated from the true velocity value but from incorrect (reduced) value of the energy diminishes proportionally to the latter. Therefore a pair of the fragments originated from conventional binary fission could reveal the mass defect similar to that characterizing a CCT event. However, if one rejects the events corresponding to the sufficient mass asymmetry determined by means of the ratio of the velocities which occurred beyond the velocity-window selected (Fig.13), the notable part of the scattered events under consideration are also discriminated automatically. This selection cuts off a part of the binary events loci due to velocity gating. Also their «scattered projections», i.e. the tails in the direction of smaller masses, disappear.

Special attention should be paid to the «rectangle» in Fig. 12 *b* which is bounded by the clusters from at least three sides. Corresponding magic numbers are marked in this figure at the bottom of the element symbols. More complicated structures (marked by the arrows *a*, *b*, *c* in Fig. 12 *c*) are observed in the mass-mass plot if the events with two fired neutron counters are also taken into play. Omitting for a moment physical treating of the structures observed, we attract attention to the specific peculiarity of some lines constituted the structures «*b*» and «*c*». The sum of the masses along them remains constant, see the dashed line in the lower left corner of Fig. 12 *c* for comparison.

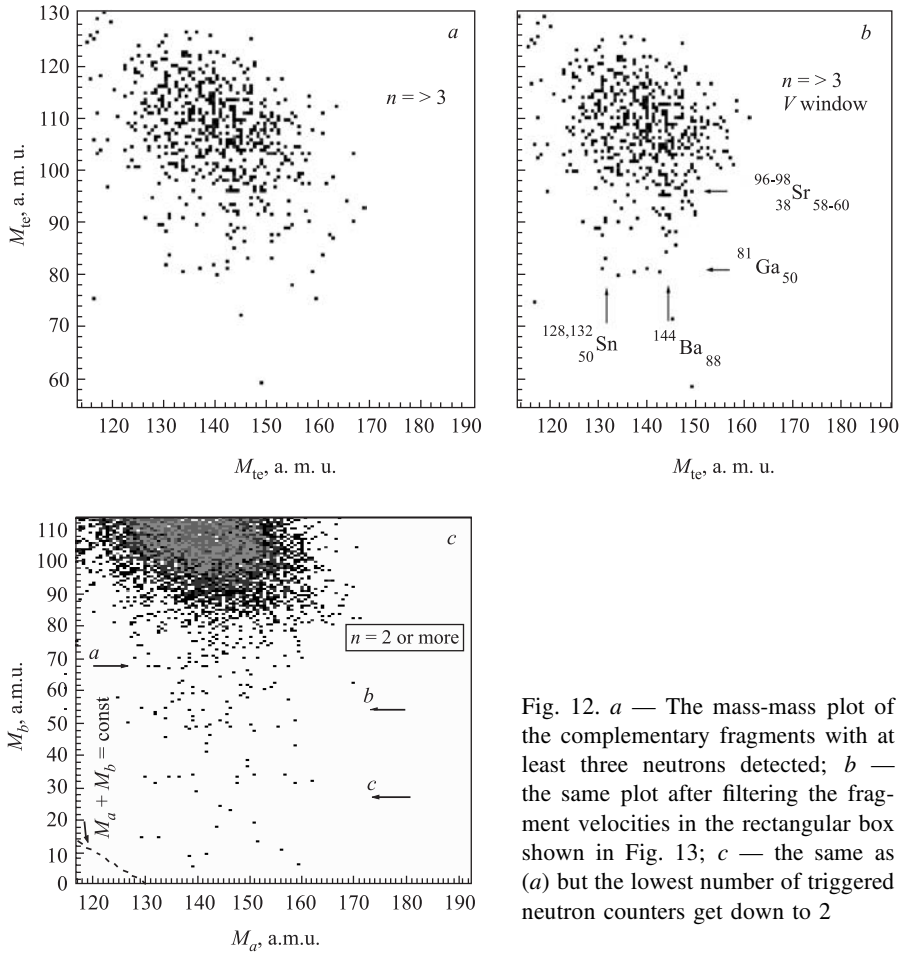

Fig. 12. *a* — The mass-mass plot of the complementary fragments with at least three neutrons detected; *b* — the same plot after filtering the fragment velocities in the rectangular box shown in Fig. 13; *c* — the same as (*a*) but the lowest number of triggered neutron counters get down to 2

Fig. 15 *a* represents a similar structure to that shown in Fig. 12 *a* except that it is not gated by neutrons and both the velocity and the momentum windows select the events in the vicinity of the mass-symmetric partitions. The corresponding momentum distribution of the fragments and the selection applied are shown in Fig. 14. The plot in Fig. 15 *b* obtained on conditions of the momentum selection solely is not so clear.

However, like in the previous case the rectangular structure (Fig. 15) observed is bounded by the magic fragments, namely ^{68}Ni (the spherical proton shell $Z = 28$ and the neutron subshell $N = 40$) and, probably, ^{84}Se (the spherical neutron shell $N = 50$). Each structure revealed maps an evolution of the decaying

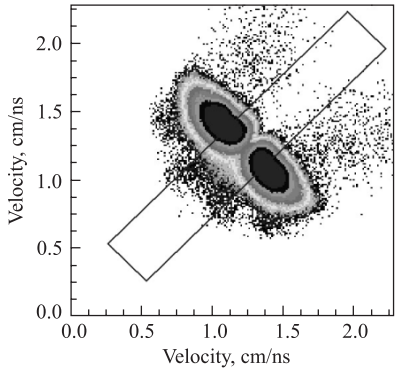

Fig. 13. Velocity matrix of complementary fragments. The events falling into the rectangular box were used to compose the final mass-mass plot in Fig. 15

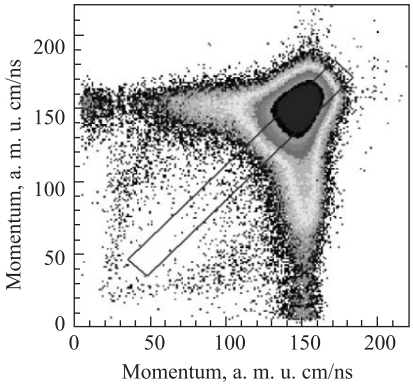

Fig. 14. Momentum-momentum plot. The events falling into the rectangular box were used to compose the final mass-mass plot in Fig. 15

system onto the mass space. Reconstruction of the evolution scenarios is a goal of the forthcoming analysis.

The events at the lower left corner of the rectangle attract special attention as they form well-separated blocks in the matrices of the experimental observables (velocity and energy). Table 2 exemplifies the parameters of three most symmetric events.

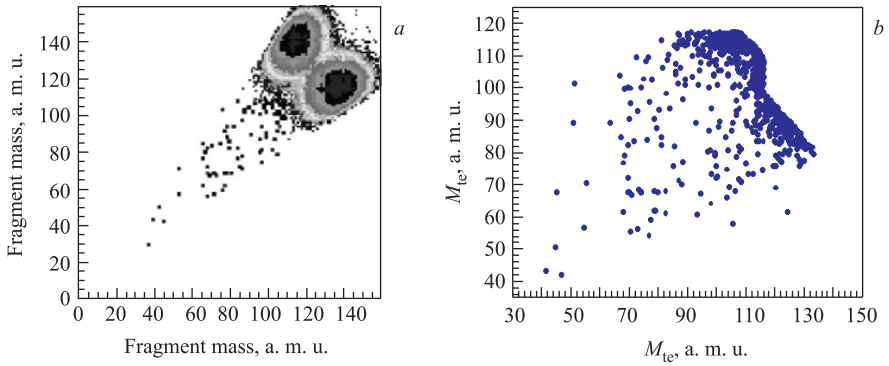

Fig. 15. The mass matrix of complementary fragments selected by two conditions requirement of their approximately equal velocities and momenta (Figs. 13, 14) (*a*), a part of the same matrix if only momentum selection is assumed (*b*)

Table 2. **Experimental parameters of the most symmetric three events**

Parameter	Event No. 1	No. 2	No. 3
Number of triggered neutron counters	0	0	1
Velocity in the arm «*a*», V_a, cm/ns	1.147	1.102	1.135
Velocity in the arm «*b*», V_b, cm/ns	1.173	1.141	1.23
TOF-TOF mass, $M_{\mathrm{tt}a}$, a.m.u.	127.4	128.2	131.1
TOF-TOF mass, $M_{\mathrm{tt}b}$, a.m.u.	124.6	123.8	120.9
Momentum P_a, cm/ns $\cdot$ a.m.u.	79.6	80.7	7.8
Momentum P_b, cm/ns $\cdot$ a.m.u.	84.7	78.3	83.4
TOF-E mass $M_{\mathrm{te}a}$, a.m.u.	69.4	73.2	69.4
TOF-E mass $M_{\mathrm{te}b}$ a.m.u.	72.2	68.6	67.8
$E_{\mathrm{te}a}$, emission energy, MeV	47.5	46.3	46.5
$E_{\mathrm{te}b}$, MeV	51.7	46.5	53.4
$\mathrm{TKE}_{\mathrm{te}}$, total kinetic energy, MeV	99.1	92.7	99.9

One can judge from Table 2 that the cluster masses obtained by the TOF-E analysis are located in the vicinity of the mass numbers 68 and 72. Both nuclei are attributed presumably to the magic Ni isotopes. The content of neutrons for the fragments whose masses are close to 72 complies then with the prediction of the unchanged charge density hypotheses. The surprising fact is that the evaluated TKE value even for very elongated imaginary chain such as Ni-C-Zn-C-Ni exceeds the experimental findings ($\sim$100 MeV). The next point to be stressed is that the observed neutron multiplicity (the number of triggered neutron counters in Table 2) is low and, hence, the number of emitted neutrons could not be high. This contradicts the expectations put forward earlier. The discrepancies reported may be an indication of more complicated decay scenario to be restored.

CONCLUSIONS

The following conclusions sum up the results:

- The multi-fragment (at least ternary) fission is experimentally confirmed;
- Clustering of the decaying system, i.e. preformation of the magic constituents inside its body, is decisive for the effect observed;
- The collinear prescission configuration predicted by theory is proved to be a preferable one for true tripartition.

The results obtained seem to be an exciting message to the people searching for unusual tripartition using the $\gamma-\gamma$ coincidence technique [17]. The events

forming rectangles in Figs. 12 and 15 should be accompanied at least by the gamma-quanta emitted simultaneously by two light fragments (for instance, ^{68}Ni and ^{82}Ge). Evidently such events are ruled out in conventional binary fission.

Acknowledgements. The authors are grateful to Dr. A. V. Daniel, Dr. N. V. Antonenko, Dr. G. G. Adamian for fruitful discussions and to Dr. I. P. Tsurin for his help in the manuscript preparation. We thank as well Prof. W. von Oertzen for very useful comments.

This work is supported in part by CRDF (grant MO-011-0).

REFERENCES

1. *Pyatkov Yu. V. et al.* // Proc. of the XIV Intern. Workshop on Nuclear Fission Physics, 12–15 October 1998, Obninsk. P. 31.
2. *Pyatkov Yu. V. et al.* JINR Preprint D15-98-263. Dubna, 1998.
3. *Pyatkov Yu. V. et al.* // Proc. of the Intern. Conf. «50 Years of Shells», 21–24 April 1999, Dubna. Singapore: World Scientific, 2000. P. 301.
4. *Ortlepp H.-G. et al.* // Nucl. Instr. and Meth. A. 1998. V. 403. P. 65.
5. *Kamanin D. V. et al.* // Physics of Atomic Nuclei. 2003. V. 66. P. 1655.
6. *Pyatkov Yu. V. et al.* // Physics of Atomic Nuclei. 2003. V. 66. P. 1631.
7. *Muga M. L. et al.* // Phys. Rev. 1967. V. 161. P. 1266.
8. *Schall P. et al.* // Phys. Let. B. 1987. V. 191. P. 339.
9. *Diehl H., Greiner W.* // Nucl. Phys. A. 1974. V. 229. P. 29.
10. *Poenaru D. N. et al.* // Proc. Symp. on Nuclear Clusters. Rauischholzhaussen, Germany, 5–9 August 2002. P. 283.
11. *Solyakin G. E. et al.* Preprint NP-50-1998. Gatchina, 1998; *Kravtsov A. V. et al.* // Phys. Rev. C. 1999. V. 60. 017601.
12. *Schmitt H. V. et al.* // Phys. Rev. 1966. V. 141. P. 1146.
13. *Prade H., Donau F.* FZR 92-09, Mai 1992.
14. *Wahl A. C. et al.* // Phys. Rev. 1962. V. 126. P. 1112.
15. *Sokol E. A. et al.* // Nucl. Instr. and Meth. A. 1997. V. 400. P. 96.
16. *Sokol E. A.* Private communication.
17. *Ter-Akopian G. M. et al.* // Phys. Rev. C. 1997. V. 55. P. 1146.

Received on April 14, 2004.

Корректор *Т. Е. Попеко*

Подписано в печать 22.06.2004.
Формат 60 × 90/16. Бумага офсетная. Печать офсетная.
Усл. печ. л. 1,43. Уч.-изд. л. 2,04. Тираж 300 экз. Заказ № 54487.

Издательский отдел Объединенного института ядерных исследований
141980, г. Дубна, Московская обл., ул. Жолио-Кюри, 6.
E-mail: publish@pds.jinr.ru
www.jinr.ru/publish/